RSC Advances

ROYAL SOCIETY OF CHEMISTRY

www.rsc.org/advances

PAPER

Continuous-flow focusing of microparticles using induced-charge electroosmosis in a microfluidic device with 3D AgPDMS electrodes

Received 00th January 20xx,
Accepted 00th January 20xx

DOI: 10.1039/x0xx00000x

www.rsc.org/

Yankai Jia [a], Yukun Ren[a]* and Hongyuan Jiang[ab]*

We herein present for the first time a microfluidic device that utilizes AC induced-charge electro-osmosis (ICEO) to continuously focus microparitcles from suspending medium. An advanced conducting silver-polydimethylsiloxane (AgPDMS) composite is chosen to fabricate three dimensional (3D) driving electrodes thereby to generate a uniform AC electric field, resulting in a vortex ICEO flow on a planar floating electrode positioned at the bottom of the main channel. The 3D electrodes are employed due to its advantage of avoiding negative effects of alternating current electro-osmosis (ACEO) and dielectrophoresis (DEP). The combination of the ICEO flow and forward flow in the device channel focuses the microparitlces in a thin stream and collects them in a specific outlet. We design the device based on the non-linear electrokinetic theory and flow field simulation, and validated the device performance under different experimental conditions including signal frequency, potential amplitude, and inlet flow rate. The highest focusing efficiency for yeast cells can reach to 96.6% at the frequency of 600Hz and the potential amplitude of 15Vp. The results provide a promising method to flow-focus microparticles in modern microfluidic systems by using ICEO.

1. Introduction

Microfluidic devices have been increasingly employed to manipulate particles due to the low sample and reagent cost, flexible integration, good analytical performance and various other advantages[1-4]. In many of these microfluidic devices, flow focusing microparticles or cells into a narrow, well-defined streams is usually a necessary step prior to counting, detecting, and sorting them, such as flow cytometry[5] and fluorescence activated cell sorting (FACS)[6]. Up to now, a variety of microparticles focusing technologies have been developed, including hydrodynamic focusing[7, 8], electrokinetic focusing[9-11], acoustic focusing[12-14] and hydrophoretic focusing[15-17] etc.. Despite of their fruitful advances, these approaches are usually limited by their respective disadvantages. For instance, although the hydrodynamic mechanism provides an effective means of accurately trapping particles into a narrow location, it still needs very strict design of the channels and precisely control of the flow rates. The acoustic focusing is another promising method to achieve this aim using very simple structures, it suits to manipulate many kinds of particles and not limited by their physical characteristics. However, this method is usually difficult to be integrated with other microfluidic systems. Moreover, magnetism is a flexible force that is often used to manoeuver particles in microfluidic devices, but it only fits for controlling magnetic particles or particles with magnetic labels, which confines its application from many non-magnetic conditions.

Electrokinetic focusing is an effective method for non-contact manipulation of particles, which mainly includes dielectrophoretic and alternating current electroosmotic(ACEO) forces [18, 19]. In this electrokinetic technique, particles are pumped through a microfluidic device and the forces are applied to the particles laterally, such that they are confined to a narrow stream. However, the dielectrophoretic methods often require complex electrode structures and strict particle size limit[20]. For the ACEO approach, the fluid flow has a large effective actuating range, and allows to trap vast particles in a short time[21-23]. Nevertheless, the ACEO flow results from the double-layer polarization on the surface of the driving electrodes, and the strongest flow happens above the driving electrodes. Therefore, this feature confined the effective range of ACEO flow, making it unable to introduce slip flow to specific spot in the electric field. Moreover, the extra links on the driving electrodes make its unfeasible to integrate with other device.

Recently, induced charge elelctroosmosis (ICEO) has emerged as a flexible tool for microparticle trapping[24]. Since ICEO flow occurs above floating electrodes, it overcomes the shortcomings of ACEO by flexible arranging floating electrodes between driving electrodes without wire connection, which makes it promising for particle focusing. In fact, ICEO has initially received great attention in the microfluidic community

[a] School of Mechatronics Engineering, Harbin Institute of Technology, West Da-zhi Street 92, Harbin, Heilongjiang, PR China 150001. E-mail: rykhit@hit.edu.cn and jhy_hit@hit.edu.cn
[b] State Key Laboratory of Robotics and System, Harbin Institute of Technology, West Da-zhi Street 92, Harbin, Heilongjiang, PR China 150001.
† Electronic Supplementary Information (ESI) available. See DOI: 10.1039/x0xx00000x

for its flexible fluid actuation ability over floating electrodes but not particle manipulation capacity[25, 26]. We first introduced this technology to obtain position-controllable trapping of particles by utilizing the ICEO advantages, such as the free floating electrodes arrangement, large effective actuating range, and efficient trapping ability. It is worth mentioning that our previous study focuses only on the static trapping analysis. In most situations, a microfluidic device that is able to focusing particle samples in continuous flow rather than a static focusing is often of particular interest.

Inspired by our previous work, we attempt to explore a flow focusing method using ICEO as shown in Figure 1(a). The basic mechanism for this design is to generate vortex flow using ICEO when the samples flow along the main channel, and then the particles are continuously focused into a narrow stream. However, if introducing a classical model (in our previous work [24]) directly for continuous-flow particle focusing manipulation, two shortcomings will arise simultaneously. First, as shown in Figure 1(b), when using planar ITO electrodes as driving and floating electrodes, counter ionic charge will accumulate on the electrode surface and cause ACEO flow directing from the electrode gap to the exciting electrodes[27]. Since the direction of the ACEO flow is opposite to that of the ICEO flow, it will undermine the effect of ICEO flow, making particles at the vicinity of the driving electrodes unable to move to the central of the microchannel. Second, since the planar electrodes give rise to a nonuniform electric field, dielectrophoretic force will form at the edges of the driving electrodes and attract the microparticles from the suspending medium to the electrodes, hence, reducing the effectiveness of the ICEO flow manipulation.

How to overcome the drawbacks of ACEO and DEP to thereby realize desired flow focusing of microparticles using ICEO? A feasible approach is to use three-dimensional (3D) exciting electrodes instead of planar electrodes in this design. As shown in Figure 1(c), if 3D electrodes in the side wall are utilized as driving electrodes, though induced double-layer (IDL) is still formed on the surface of the driving electrodes, there is no tangential field components exerting on the ionic charge in the diffuse double-layer, hence the above issue on ACEO sweeping particles to the vicinity of driving electrodes will no longer exist. In addition, the face-to-face configuration of the driving electrodes introduce an uniformity AC field (no field gradient) across the main channel, so no DEP will be brought in. For fabricating appropriate 3D electrodes, a novel kind of composite material named AgPDMS is employed because of its low cost, convenience for fabrication and ease for bonding. This AgPDMS material has been validated by different groups[28-30].

In this work, we present a novel microfluidic device using ICEO flow generated above a floating metallic strip placed in the bottom of the microchannel, exploited for flow focusing of bio-particles in the suspending medium. The vortex ICEO flow is generated by an AC electric field energized by 3D face-to-face sidewall electrodes. The particles in the medium were transported through the microchannel, and brought to the central of the microchannel by ICEO flow when passing through the metallic strip. The combination of the forward transporting flow and ICEO flow give rise to the focusing of the particles (Figure 1(a)). The key advantages of this approach are the capabilities to manipulate particles away from the energized electrodes, and to focusing particles in a continuous manner. We report the fabrication of the focusing device using photolithographic method in four consecutive steps. A numerical model was built using ICEO theory to simulate the induced flow in the microchannel. The approach is validated by focusing yeast cells from low density to high density. To the authors' knowledge, this is first study that utilizes ICEO flow to continuously focus microparticles in a microfluidic device.

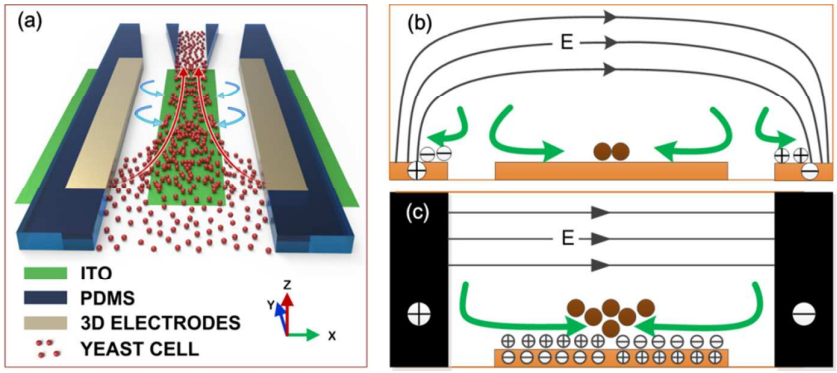

Figure 1. (a) Schematic illustration of the microchip and focusing principle: randomly distributed microparticles come into the focusing zone, focus to the central of the mainchannel and flow into the middle outlet. (b) When planar electrodes are used as energizing electrodes, ACEO flow on the planar electrodes undermines the effect of ICEO on the floating electrodes, hence decreasing the focusing efficiency. (c) Three-dimensional electrodes configured in the sidewall give rise to a uniform AC electric field, and avoid the negative impacts of the ACEO and dielectrophoresis.

2 Methods and materials

2.1 Device design and fabrication

The microfluidic chip is composed of a main channel and four branch channels, as shown in Figure 2(a). The four branch channels are connected to four respective reservoirs--the inlet, outlet A, outlet B and outlet C. An ITO (Indium-tin oxide) strip is placed at the bottom of the main channel, with two 3D face-to-face AgPMDS electrodes located at the sidewalls. The 3D electrodes are linked to outer AC source through ITO leads. All the channels are 60 µm high, and some other major dimensions for this configuration are shown in Figure 2(b). The inlet and outlets all have 6mm in height and 6mm in diameter, giving rise to a volumetric capacity of about 170 µL. Under such capacity, the liquid level difference between the inlet and outlets is able to drive a steady flow for about 15 minutes in the main channel. The principal of particle focusing is shown in Figure 1. A sample suspended with microparticles is first introduced to the inlet. An AC signal, energizing to the 3D electrodes through ITO leads, provides an AC electric field in the main channel. ICEO vortex flow is then formed above the ITO strip, which drags the particles from the surrounding medium to the bottom central of the floating electrodes. While being accumulated to the middle of the main channel, the particles would also be driven to outlet A by the forward flow, thereby collecting the dispersed particles to outlet A.

The device was fabricated following the similar procedures as presented in our previous work[29]. In brief, the fabrication procedure consists of four steps as shown in Figure 2(c): ITO leads etching, 3D electrodes patterning, PDMS channel processing, and alignment and bonding. First, a clean ITO glass slide was laminated by negative dry-film resist (Riston SD238, Dupont, USA), followed by a photolithograph process. The slide with patterned dry film was submerged into an etching solution to obtain the ITO floating electrode and leads, and then the dry film was stripped off by $NaCO_3$ solution. After that, the slide was then laminated by two layers of dry film, followed by another photolithograph process, hence generating the dry-film mold. AgPDMS gel was then filled into the dry-film mold to form the 3D electrodes. Figure 2(d) shows the SEM image of the 3D AgPDMS electrodes on a glass slide. After the generation of 3D electrodes, a PDMS slab was fabricated using conventional softlithographic method[31]. Finally, the PDMS slab and the substrate were aligned under an optical microscope and bonded together by oxygen plasma treatment. It is noted that the top surface of the 3D electrodes are bonded to the PDMS slab, while the side face-to-face surfaces severs as working surfaces.

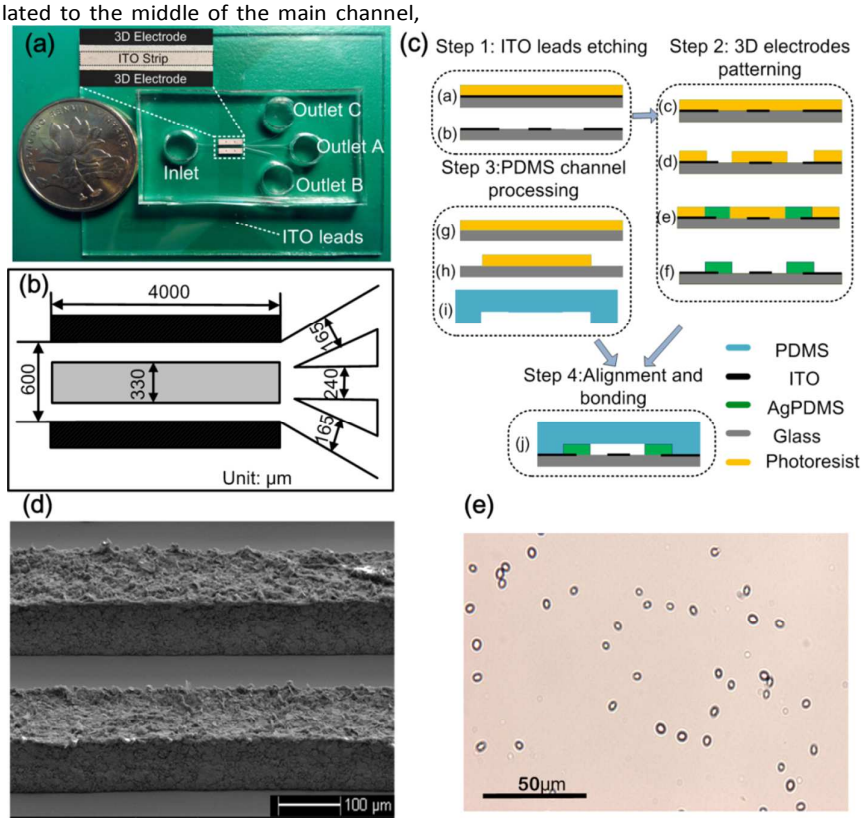

Figure 2 (a) Microfluidic chip with integrated 3D AgDPMS electrodes in the sidewall. The ITO leads were connected to an AC function generator. The inset indicates the top-view configuration of the 3D driving electrodes and the ITO floating electrode. (b) The fabrication process of the device. (c) Key dimensions of the design. (d) SEM image of the 3D AgPDMS electrodes on a glass slide before bonding with PDMS slab. (e) Micrograph of the activated yeast cells in suspending medium.

2.2 Theoretical background and flow field simulation

The bulk AC electric field acting on its own induced diffuse-charge in the Debye layer gives rise to a pair of counter-rotating ICEO vortices on the surface of the floating electrode[25]. The time-averaged ICEO slip velocity on the metallic strip surfaces is derived from the generalization of Helmho-Smoluchowski formula[25, 26]:

$$\left\langle \boldsymbol{u}_{slip} \right\rangle = \frac{1}{2}\frac{\varepsilon_f}{\eta}\frac{1}{1+\delta}\mathrm{Re}\left(\left(\tilde{\phi}-\tilde{V}_0\right)\left(\tilde{\boldsymbol{E}}-\tilde{\boldsymbol{E}}\cdot\boldsymbol{n}\cdot\boldsymbol{n}\right)^*\right) \quad (1)$$

where <·> denotes the time-average operation, Re(·) the real part of (·), * the complex conjugate operator, $\tilde{}$ the symbol of phasor amplitude, ε_f the liquid permittivity, and $\eta = 0.001\ \mathrm{Pa\cdot s}$ is the dynamic viscosity of aqueous media. Furthermore, $\boldsymbol{E}_t = \left(\boldsymbol{E}-\boldsymbol{E}\cdot\boldsymbol{n}\cdot\boldsymbol{n}\right)$ is the tangential field component on the electrode surface. $\zeta = \frac{1}{1+\delta}\left(V_0-\phi\right)$ is the induced zeta potential that contributes to induced electrokinetic flows, and δ denotes the surface physical capacitance ratio of the diffuse double-layer. When considering the physical process of induced double layer, the AC field needs a characteristic charging time to accumulate the ionic charge, and thereby developing the ionic charge cloud. For field frequency beyond the surface-averaged RC charging frequency $f_{RC-average} = \sigma_f\left(1+\delta\right)/2\pi C_d\left(0.25L\right) = 100Hz$ (L=330 μm is the width of the floating electrode) for the equivalent circuit of the liquid resistance in series with the double-layer capacitance, a spectrum of charging modes leads to a nonlinear ICEO slip profile on the electrode surface and hence generating two counter-rotating vortices as mentioned above.

For the prediction of particle focusing, the flow field on the transverse section of the main channel is numerically simulated using commercial FEM software package (COMSOL Multiphysics, v4.4). Figure 3(a) shows the simulated flow field at 600Hz and 15Vp on the right half transverse section of the main channel. The ICEO flow rate peaks at the edge of the metallic strip and decreases rapidly from the edge to the central of the ITO strip. Flow vortex forms above the surface of the floating electrode. Particles suspending in the medium would be transported constantly from the bulk liquid towards the central bottom of the microchannel by the vortices. Since the vortex flow is weak at the central of the floating electrode, particles that directed to this region would stagnate, which gives rise to a stagnant region. While drawn from the bulk medium to the central of the metallic strip, the particles are transported forward at the same time by a laminar flow from the inlet to the outlets The combination of the particle motions from the edge to the central of the floating electrode and the motion from the inlet to the outlet contributes to the continuous focusing of particles, and finally moving into outlet A.

Three-dimensional AgPDMS electrodes rather than planar ITO electrodes are utilized as the driving electrodes, so as to avoid unexpected ACEO flow and DEP that hindering the focusing process. Another simulation with planar driving electrodes is performed to compare the difference of flow field with 3D driving electrodes. For ACEO flow, when the driving flow is 3D electrodes as shown in Figure 3(a), the electric field between the channel walls is uniform and the electric field has no tangential component on the 3D electrodes, and thus there is no ACEO flow. However, if using planar electrodes as driving electrodes (Figure 3(b)), a nonuniform electric field is generated and ACEO flow appears on the planar electrodes. When considering the simultaneous charging of induced double-layer (IDL) on the surface of both the planar driving electrodes and the floating electrode of non-negligible size, the physical process is much more complicated. Direct numerical simulation of RC charging process, ACEO flow near the driving electrode pair and ICEO flow around the floating electrode is preferred and conducted. From Figure 3(d), in the frequency range of 300Hz~600Hz, flow velocity of ACEO vortex above the driving electrodes is faster than that of ICEO vortex above the floating electrode. ACEO flow tends to sweep particles from the electrode gap region to the surface of the driving electrode, in competition with ICEO flow that transports particles from the gap area to the surface of the floating electrode. Consequently, a portion of particles will move into the side branches due to the action of ACEO eddies near the planar driving electrodes, resulting in a decrease in particle focusing efficiency into the middle branch.

It is known that in non-uniform electric field dielectrophoresis (DEP) can occur over polarizable surfaces. The simulated distribution of DEP velocity is shown in Figure 3(d). The DEP velocity has the same direction with the ICEO flow at the stagnant region, but with a neglectable order of 10nm/s.

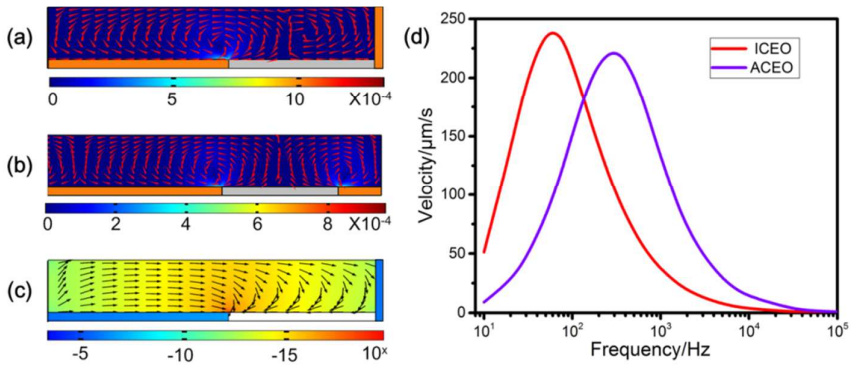

Figure 3 Numerical simulation results: (a) transverse flow field in the design with 3D electrodes; (b) transverse flow filed in the main channel if the energizing electrodes are planar electrodes; (c) Distribution of dielectrophoretic velocity in the main channel, in image (a) (b) and (c) the color difference represents the magnitude of the flow field while the arrows denote the direction of the flow field; (d) Averaged slip velocity of ICEO and ACEO above the floating electrode and the energizing electrodes, respectively, for the model shown in (b).

2.3 Sample preparation and focusing efficiency estimation

Yeast cells were obtained from Baker's dry yeast by reactivation. First, 50mg of Baker's dry yeast was introduced into 10mL DI water at 30°C. After 1h, 1mL of the yeast suspension was transferred to a centrifuge tube, and then the yeast cells were centrifuged and washed for three times using DI water. Then, 1mL of KCl solution with conductivity of 10μS/cm was added into the tube. The KCl solution with yeast cells was then diluted for 50 times for experimental use. A micrograph of the activated yeast cells in the suspending medium is shown in Figure 2(e). It is noted that, prior to each experiment, the microchannels were soaked with 5% bovine serum albumin (BSA) solution for 2h to prevent adhesion of yeast cells to the channel walls.

The AC sinusoidal signal to induce electric field was generated by a function generator (TGA12104, TTi, UK), amplified by an amplifier (Model2350, TEGAM, USA) and monitored by an oscilloscope (TDS2024, Tektronix, USA). The motion of the yeast cells was observed under an optical microscope (BX53, Olympus, Japan) and recorded using a CCD camera (RETIGA2000R, Qimaging, Canada). The focusing efficiency in this work was calculated as

$$\eta = (1 - \frac{N_{\text{loss}}}{N_{\text{inlet}}}) \times 100\% \quad (2)$$

where N_{inlet} is the number of the cells flowing from the inlet per minute, and N_{loss} refers to the number of the cells flowing into the wrong outlets—outlet B and outlet C. Each experimental is repeated three times to calculate the average focusing efficiency.

3 Results and discussion

The goal of this work is to continuously focus bioparticles dispersed in the medium to a well-defined narrow stream, and then collecting them to a specific outlet. In order to achieve effective particle focusing, three requirements must be satisfied: 1) a stagnant flow region is generated by the ICEO vortices above the central of the metallic strip; 2) the ICEO flow is strong enough to drag the particles from the bulk to the stagnant region; 3) the forward flow and the ICEO flow are well matched so that the particles have enough time to move from the bulk medium to the central of the strip. The focusing approach is validated by focusing yeast cells under different experimental conditions. The favorable conditions for the process are established by studying the effects of signal frequency, potential amplitude and inlet flow rate on focusing efficiency.

3.1 Frequency dependence

The performance of the device was first demonstrated by focusing yeast cells at different frequencies. Figure 4 shows the focusing process of yeast cells at the frequency of 600Hz and potential amplitude of 15V. Without AC signal as shown in Figure 4(a), when introducing the medium to the main channel, the yeast cells flowed randomly into the three outlets. According to the width of the outlet branches, 42% of the cells transported into outlet A. After energizing the AC signal, the yeast cells were gradually accumulated by the vortices to the central region of the strip. As time lapsed, the stagnant region became thinner and thinner. Finally, over 95% of the yeast cells flowed into outlet A.

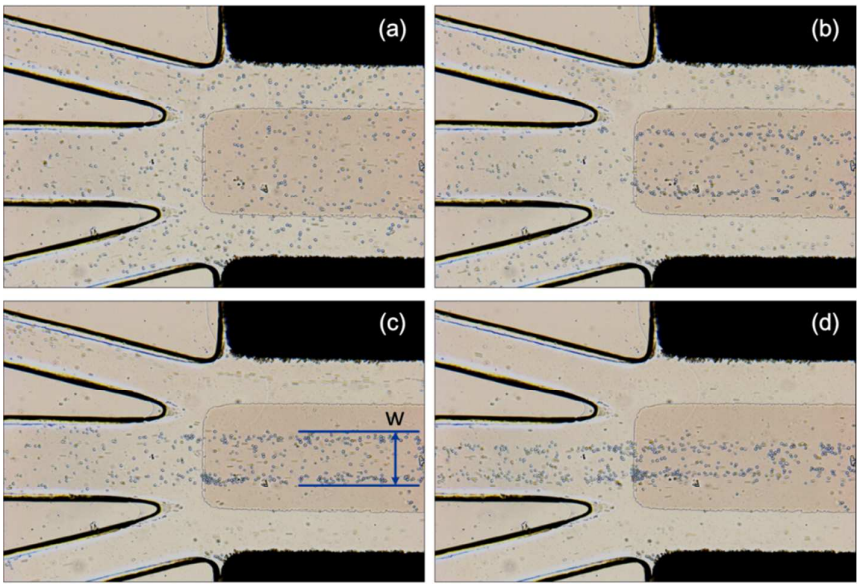

Figure 4 Time-lapse images of yeast cells focused from the medium at a frequency of 600Hz and a potential amplitude of 15V. (a) t=0s; (b) t=10s; (c) t=16s; (d) t=30s.

Figure 5 represents the particle focusing efficiency (red line) and the stagnant width (blue line) at different frequencies. Under different frequency, the cells accumulated at different stagnant width W (Figure 4(c)), hence affecting the focusing efficiency. In order to obtain steady focusing, the upward ICEO flow should be balanced by the particle buoyancy force[24], so the experiments were attempted at the frequency $f \geq f_{RC-average}$. At 100Hz, the stagnant width was 80μm with the focusing efficiency of 76.1%. The stagnant region was narrow because the ICEO velocity was strong at the edges of the strip and decayed gradually toward the central of the electrode, as presented by the simulated slip profile in Figure 5(b). Since the upward flow velocity was also strong at the stagnant region, many cells followed the circulating vortices and were brought back to the outer region of the floating electrode. These cells were likely to move into outlet B or outlet C, which leads to low focusing efficiency at this frequency. When increasing the frequency to 300Hz, the ICEO slip velocity declined at the edges of the ITO electrode and the decayed more quickly than lower frequency from the edges to the middle of the ITO electrode, as shown in Figure 5(b). A wider stagnant region of 83.3 μm and a focusing efficiency of 94.8% were obtained. The efficiency continued to grow with the increase of the frequency, and peaked at 600Hz, reaching to 96.6%. This frequency was experimentally verified the optimal for continuous cell focusing at a specific applied voltage in this device. A possible reason for the missing cells is the DEP effect arising from the driving electrodes. As Figure 2(d) shows, the side surface of the 3D electrodes is not very smooth where the roughness may cause local field gradient, the yeast cells, experiencing pDEP, are likely to be attracted at the sharp point of the 3D electrodes. It is noted that, as elaborated in section 2.2, the DEP effect using 3D AgPDMS is relative tiny compared to that by using planar electrodes.

As Figure 5(b) shows, when increasing the frequency from 600 Hz to 2 KHz, the slip velocity declined rapidly thereby reducing the ICEO flow vortices dramatically. Therefore, fluid drag force on the cells away from the floating electrode was not strong enough to take them to the central of the ITO strip. For the maximum experimental frequency of 2 KHz, the stagnant width increased to 232 μm, while the focusing efficiency was only 89.4%.

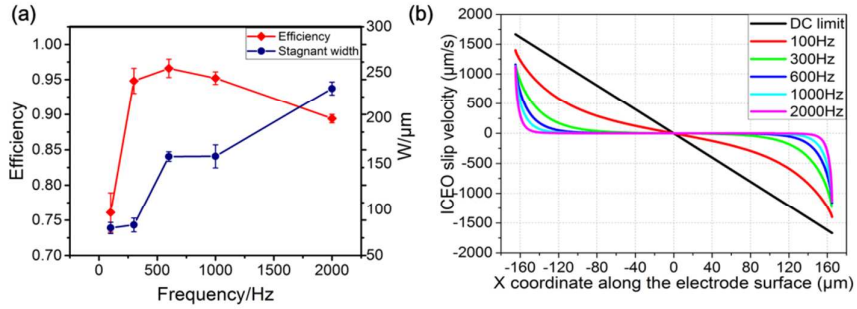

Figure 5 (a) Particle focusing efficiency and stagnant width at different frequencies; (b) Simulated ICEO slip velocity on the floating electrde at different frequencies.

3.2 Potential amplitude

The amplitude of the AC sinusoidal potential is another key parameter that affects the focusing process. We varied the

strength of the applied potential amplitude in our experiments from 7.5 V to 17.5V. It is clear that the stagnant width decreases on increasing the voltage because of the strong ICEO vortex driving, thereby, raising the focusing efficiency. Experimental images for the focusing of particles at two different potential amplitudes, 7.5V and 12.5V, are compared in Figure 6. At the amplitude of 7.5 V (Figure 6(a)), the stagnant width was 188 µm. Although most of the particles were contained in the stagnant band, some particles still flowed to the side outlets, resulting from the insufficient vortices because of the low voltage support. The focusing efficiency was 86.4% under this condition. In contrast, at the amplitude of 12.5 V (Figure 6(b)), the stagnant width decreased to 175 µm and the focusing efficiency was increased to 94.1%.

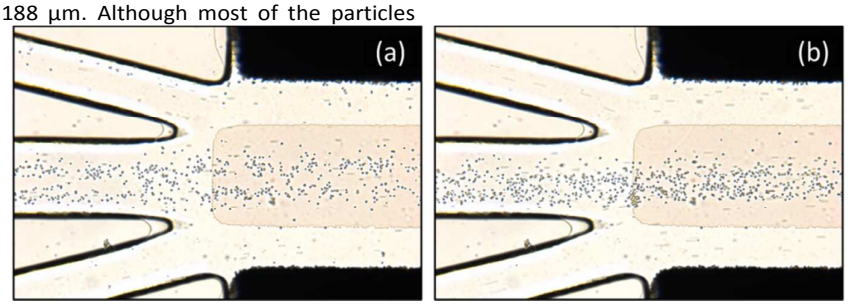

Figure 6 Focusing of yeast cells at 600Hz of different voltages: (a) 7.5 V and (b) 17.5 V.

Figure 7(a) shows the stagnant width and focusing efficiency varying with potential amplitude from 7.5V to 17.5V. The maximum focusing efficiency happened at 17.5V with the stagnant width of 118 µm. Bubbles on the energized electrodes arose when the potential amplitude increased beyond 17.5 V. The simulated slip velocity profile accounts for the focusing patterns at different potential amplitudes, as shown in Figure 7(b). The maximum slip rate occurred at the edges of the floating electrode, and the flow rate decayed rapidly from the edges to the central of the floating electrodes. Meanwhile, the maximum flow rate increased with the increasing potential amplitude. A stronger slip flow led to stronger vortices, which directed more particles to the stagnant region and resulted higher efficiency.

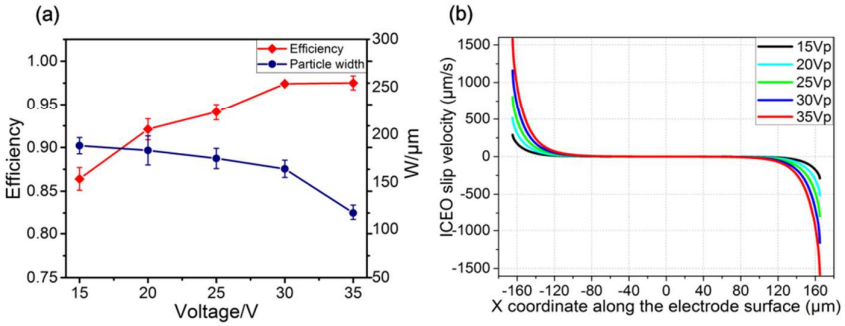

Figure 7 (a) Particle focusing efficiency and stagnant width at different potential amplitudes; (b) Simulated ICEO slip velocity on the floating electrde at different frequency.

3.3 Inlet flow rate

The effect of forward flow rate on focusing efficiency was studied at the signal frequency of 600Hz and potential amplitude of 15V. Since the volume of the reservoirs was capable of giving a steady flow for 15 minutes, the focusing efficiency was calculated at different time after inducing the solution with particles, which represented the focusing efficiency for different flow rates. The efficiencies were counted at the second minute, the fourth minute, the sixth minute, the eighth minute and the eleventh minute. Figure 8 demonstrates the particle focusing images at the second minute and the eighth minute. With fast forward flow, the duration time for particles being transported from the bulk to the middle of the floating electrode was short, so the stagnant region was wide, resulting in a low efficiency. As shown in Figure 8(a), at the second minute, the stagnant width was 268 µm and the focusing efficiency was 84%. The efficiency was low because the fast flow did not provide enough for the particles to accumulate to the middle of the ITO strip. In contrast, at the eighth minute, most of the particles were transported to the middle of the floating electrode by the vortices, with a stagnant width of 192 µm and an efficiency of 95%. In Figure 9, the relationships of flow rate with stagnant width and focusing efficiency were clearly shown: the stagnant width decreased with the decreasing flow rate, while the focusing efficiency increased with the decreasing flow rate.

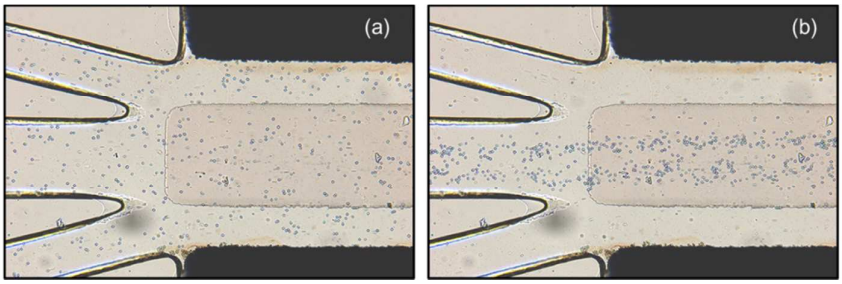

Figure 8 Focusing of yeast cells at 600Hz of different flow rates: (a) second minute; (b) eight minute.

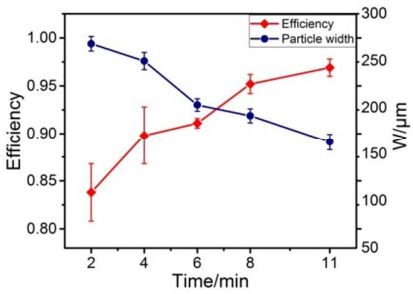

Figure 9 Particle focusing efficiency and stagnant width at different inlet flow rate.

3.4 Potential impact of Joule heating and electric field on particle focusing

Non-uniform Joule medium heating above electrode surfaces can result in temperature elevation and hence electrothermal flow (ETF) in the electrolyte bulk, which can affect particle focusing at a sufficient liquid conductivity. However, at the experimental liquid conductivity level 0.001 S/m, ETF induced by Joule heating is negligible small (10 nm/s) by numerical simulation and therefore would not affect particle focusing in the experiments. Besides, even if the liquid conductivity reaches 1 S/m, the ETF flow rate is only about 1 μm /s, and the corresponding maximum temperature elevation is merely 1.04 K inside the liquid medium, so the effect of ETF on particle focusing can be ignored in this device.

Electric field may also directly affect cells by imposing a transmembrance voltage on cells[32]. The maximum amplitude of electric field intensity in the experiments is $E = U_{rms}/d = (17.5/\sqrt{2})\ \mathrm{V}/0.6\ \mathrm{mm} = 20.6\ \mathrm{kV/m}$. Here U_{rms} is the maximum root-mean-square voltage applied to the sidewall electrodes, d is the gap distance between the driving electrodes. According to Ref.[32], at DC a 10μm mammalian cell in a 10 kV/m field will incur a 75 mV imposed potential, approximately equal to the endogenous potential. Although the field amplitude 20.6 kV/m in our experiments is stronger than 10 kV/m, the field frequency 600 Hz remarkably reduced the induced potential on cells to lower than 75 mV. What's more, since yeast cells own cell walls, they are more tolerable in the electric field. Therefore, the viability of yeast cells would not be affected by electric field.

4 Conclusions

We have developed a microfluidic device for continuous focusing of target particles from suspending medium by using the combined effect of ICEO vortex flow and forward flow. The design uses 3D AgPDMS electrodes to provide a uniform AC electric field, and planar ITO electrode as floating electrode. The performance of the device was validated by continuously focusing yeast cells to a specific outlet. Moreover, the effects of different experimental conditions were investigated including the signal frequency, potential amplitude and input flow rate. The experimental results reveal that the focusing efficiency is increased by (i) increasing the signal frequency blow 600 Hz, or (ii) increasing the applied voltage, while decreased by (i) increasing the signal frequency beyond 600 Hz, or (ii) increasing the input flow rate. It's worth mentioning that this configuration overcomes the negative effects of ACEO and DEP arising from the driving electrodes. Additionally, the highest efficiency of this design reaches to 96.6% at the frequency of 600 Hz and potential amplitude of 15 Vp. Given its good performance and unique advantages, the design has great potential for sample focusing and collecting, and integrating with other lab-on-a-chip components to realize sophisticated applications.

Acknowledgements

The authors gratefully acknowledge the National Natural Science Foundation of China (No.51305106 and No. 11372093), the Fundamental Research Funds for the Central Universities (Grant No. HIT. NSRIF. 2014058 and Grant No. HIT. IBRSEM. 201319).

Notes and references

1. E. K. Sackmann, A. L. Fulton and D. J. Beebe, *Nature*, 2014, **507**, 181-189.
2. G. M. Whitesides, *Nature*, 2006, **442**, 368-373.
3. T. M. Squires and S. R. Quake, *Reviews of modern physics*, 2005, **77**, 977.
4. L. Y. Yeo, H. C. Chang, P. P. Chan and J. R. Friend, *small*, 2011, **7**, 12-48.
5. C. Simonnet and A. Groisman, Analytical chemistry, 2006, 78, 5653-5663.
6. A. Wolff, I. R. Perch-Nielsen, U. Larsen, P. Friis, G. Goranovic, C. R. Poulsen, J. P. Kutter and P. Telleman, *Lab on a Chip*, 2003, **3**, 22-27.
7. D. Di Carlo, D. Irimia, R. G. Tompkins and M. Toner, Proceedings *of the National Academy of Sciences*, 2007, **104**, 18892-18897.
8. M. G. Lee, S. Choi and J.-K. Park, *Lab on a Chip*, 2009, **9**, 3155-3160.
9. C. Yu, J. Vykoukal, D. M. Vykoukal, J. A. Schwartz, L. Shi and P. R. Gascoyne, *Microelectromechanical Systems, Journal of*, 2005, **14**, 480-487.
10. H. Chu, I. Doh and Y.-H. Cho, *Lab on a Chip*, 2009, **9**, 686-691.
11. J. Zhu, T.-R. J. Tzeng, G. Hu and X. Xuan, *Microfluidics and* nanofluidics, 2009, **7**, 751-756.
12. J. Shi, X. Mao, D. Ahmed, A. Colletti and T. J. Huang, *Lab on a Chip*, 2008, **8**, 221-223.
13. M. E. Piyasena, P. P. Austin Suthanthiraraj, R. W. Applegate Jr, A. M. Goumas, T. A. Woods, G. P. López and S. W. Graves, *Analytical chemistry*, 2012, **84**, 1831-1839.
14. H. Li, J. R. Friend and L. Y. Yeo, *Biomedical microdevices*, 2007, **9**, 647-656.
15. S. Choi and J.-K. Park, *Analytical chemistry*, 2008, **80**, 3035-3039.
16. S. Song and S. Choi, *Applied Physics Letters*, 2014, **104**, 074106.
17. S. Yan, J. Zhang, M. Li, G. Alici, H. Du, R. Sluyter and W. Li, Scientific *reports*, 2014, **4**.
18. H. Morgan and N. G. Green, *AC electrokinetics: colloids and* nanoparticles, Research Studies Press, 2003.
19. A. Ramos, *Electrokinetics and electrohydrodynamics in* microsystems, Springer Science & Business Media, 2011.
20. R. Pethig, *Biomicrofluidics*, 2010, **4**, 022811.
21. J. Wu, Y. Ben, D. Battigelli and H.-C. Chang, *Industrial &* engineering *chemistry research*, 2005, **44**, 2815-2822.
22. K. H. Bhatt, S. Grego and O. D. Velev, *Langmuir*, 2005, **21**, 6603-6612.
23. E. M. Melvin, B. R. Moore, K. H. Gilchrist, S. Grego and O. D. Velev, *Biomicrofluidics*, 2011, **5**, 034113.
24. Y. Ren, W. Liu, Y. Jia, Y. Tao, J. Shao, Y. Ding and H. Jiang, *Lab* on *a* Chip, 2015, **15**, 2181-2191.
25. T. M. Squires and M. Z. Bazant, *Journal of Fluid Mechanics*, 2004, **509**, 217-252.
26. M. Z. Bazant and T. M. Squires, *Current Opinion in Colloid & Interface* Science, 2010, **15**, 203-213.
27. D. Li, *Encyclopedia of microfluidics and nanofluidics*, Springer Science & Business Media, 2008.
28. X. Z. Niu, S. L. Peng, L. Y. Liu, W. J. Wen and P. Sheng, *Advanced* Materials, 2007, **19**, 2682-2686.
29. Y. Jia, Y. Ren and H. Jiang, ELECTROPHORESIS, 2015.
30. N. Lewpiriyawong, K. Kandaswamy, C. Yang, V. Ivanov and R. Stocker, Analytical *chemistry*, 2011, **83**, 9579-9585.
31. Y. Xia and G. M. Whitesides, *Annual review of materials science*, 1998, **28**, 153-184.
32. J. Voldman, *Annu. Rev. Biomed. Eng.*, 2006, **8**, 425-454.